THE JOURNAL OF PHYSICAL CHEMISTRY C

Article

Cite This: J. Phys. Chem. C 2019, 123, 8439−8446

pubs.acs.org/JPCC

CO_2 Adsorption on $Ti_3O_6^-$: A Novel Carbonate Binding Motif

Sreekanta Debnath,[†,‡] Xiaowei Song,[‡] Matias R. Fagiani,[†,‡] Marissa L. Weichman,[§,∥] Min Gao,[⊥,#] Satoshi Maeda,[#,○] Tetsuya Taketsugu,[#,○,□] Wieland Schöllkopf,[‡] Andrey Lyalin,[*,□] Daniel M. Neumark,[*,§,△] and Knut R. Asmis[*,†]

[†]Wilhelm-Ostwald-Institut für Physikalische und Theoretische Chemie, Universität Leipzig, Linnéstrasse 2, D-04103 Leipzig, Germany

[‡]Fritz-Haber-Institut der Max-Planck-Gesellschaft, Faradayweg 4-6, D-14195 Berlin, Germany

[§]Department of Chemistry, University of California, Berkeley, California 94720, United States

[⊥]Institute for Catalysis, Hokkaido University, Sapporo 001-0021, Japan

[#]Department of Chemistry, Faculty of Science, Hokkaido University, Sapporo 060-0810, Japan

[○]Institute for Chemical Reaction Design and Discovery (WPI-ICReDD), Hokkaido University, Sapporo 001-0021, Japan

[□]Global Research Center for Environment and Energy based on Nanomaterials Science (GREEN), National Institute for Material Science (NIMS), Tsukuba 305-0044, Japan

[△]Chemical Sciences Division, Lawrence Berkeley National Laboratory, Berkeley, California 94720, United States

Supporting Information

ABSTRACT: CO_2 adsorption on $Ti_3O_6^-$, which serves as a model for an oxygen vacancy on a titania surface, is studied using infrared photodissociation (IRPD) spectroscopy in combination with density functional theory (DFT) and coupled cluster computations, as well as a recently developed multicomponent artificial force induced reaction method. The IRPD spectra of D_2-tagged $[(Ti_3O_6)(CO_2)_n]^-$, with n = 1, 2, are reported in the spectral window of 450−2400 cm^{-1} and assigned based on a comparison to harmonic IR spectra from the DFT calculations. We find that CO_2 binding leaves the unpaired electron largely unperturbed. The first two CO_2 molecules adsorb chemically to $Ti_3O_6^-$ by incorporating a formally doubly negatively charged, either doubly or triply coordinated O atom to form a bidentate or tridentate bridging carbonate dianion (CO_3^{2-}), respectively. The latter binding motif exhibits a characteristic IR signature in the form of an intense doublet of peaks near 1400 cm^{-1} stemming from two antisymmetric carbonate stretching modes.

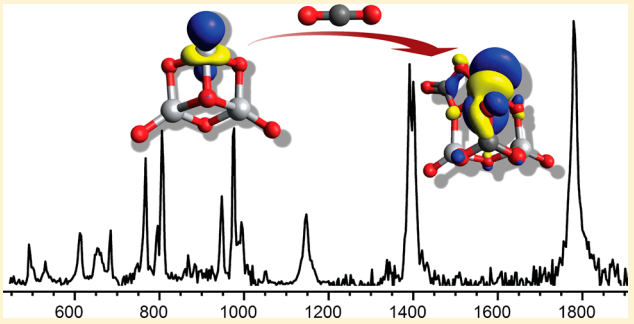

1. INTRODUCTION

Steadily growing global energy consumption has led to a sharp rise in atmospheric CO_2 levels, one of the factors contributing to anthropogenic climate change. Hence, there is an increasing demand for efficient methods to reduce atmospheric CO_2 and convert it into value-added chemicals using heterogeneous catalysts.[1,2] TiO_2-based materials have been identified as promising, cost-efficient candidates for CO_2 sequestration and conversion, considering their relative abundance in earth's crust in combination with their photocatalytic activity.[3−5] To enhance the photocatalytic efficiency, it is necessary to develop an understanding of the fundamental processes occurring at the TiO_2 interface. Adsorption studies of CO_2 on titania, for example, have focused on a molecular level characterization of chemi- versus physisorption, that is, formation of bicarbonate or carbonate versus CO_2 binding exclusively to a metal center through one of its oxygen atoms, and are typically discussed in the context of Lewis acids and bases, finding that stronger CO_2 binding is promoted by higher oxygen basicity as well as higher metal acidity.[6−9] Here, we employ a complementary approach to shed new light on TiO_2−CO_2 interactions. We use infrared photodissociation (IRPD) spectroscopy, combined with density functional theory (DFT) calculations, to study CO_2 adsorption by the radical anion $Ti_3O_6^-$ in the gas phase. This cluster represents a model for oxygen vacancies on titania surfaces.[10] The goal of the present study is identifying the vibrational signatures of characteristic binding motifs in the vicinity of such defect sites.

The C_s structure of $Ti_3O_6^-$ (see Figure 1), characterized previously by IRPD spectroscopy,[10] exhibits two 4-fold coordinated Ti^{4+} centers and one triply coordinated Ti^{3+}

Special Issue: Hans-Joachim Freund and Joachim Sauer Festschrift

Received: November 3, 2018
Revised: December 7, 2018
Published: December 12, 2018

DOI: 10.1021/acs.jpcc.8b10724
J. Phys. Chem. C 2019, 123, 8439−8446

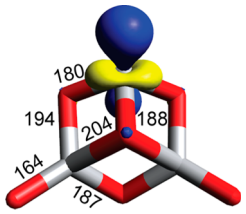

Figure 1. Spin density plot of the singly occupied molecular orbital in the $Ti_3O_6^-$ anion from ωB97XD/aug-cc-pVTZ calculations. The unpaired electron is localized at the under coordinated Ti^{3+} center. Bond lengths (in pm) are also shown.

center. The latter carries the spin density and represents the reactive center for hydrogen dissociation[11] as well as water adsorption.[12] CO_2 adsorption could be favorable at this site as it represents an electron donor site for the π acceptor CO_2. However, there are many possible binding motifs known from CO_2 adsorption studies on titania surfaces[7,8,13,14] and on neutral and small anionic titanium oxide clusters in the gas phase.[15,16] These include chemisorbed monodentate, bridging bidentate, chelating bidentate and tridentate carbonates, oxalates, as well as configurations with linear and bent physisorbed CO_2. A priori, it is unclear which binding motifs are preferred in the $[Ti_3O_6(CO_2)_n]^-$ system. Our results show that two types of tridentate carbonates, each with its own characteristic IR signature, are formed, an asymmetric and a symmetric one, of which the latter has not been reported previously.

2. EXPERIMENTAL AND COMPUTATIONAL METHODS

Experimental Methods. The IRPD experiments were carried out with an ion trap tandem mass spectrometer described previously.[17,18] In brief, $[Ti_3O_6(CO_2)_n]^-$ (n = 1, 2) clusters are produced in a dual gas channel pulsed laser-vaporization source operated at 50 Hz.[11,19] The beam of ions passes through a 4 mm diameter skimmer and is collimated in a radio frequency (RF) decapole ion-guide filled with He buffer-gas. Ions of interest are mass-selected according to their mass/charge ratio using a quadrupole mass-filter (see Figure S1 for a characteristic mass spectrum of the $[Ti_3O_6(CO_2)_n]^-$ clusters studied here). The mass-selected beam is focused into a cryogenically cooled RF ring-electrode ion trap. The trap is continuously filled with buffer gas (10% D_2 in He) at a trap temperature of 13−15 K, which allows for the accumulation and thermalization of the trapped ions. Inside the trap, ions undergo three-body collisions with the buffer gas, which promote the formation of weakly bound ion-D_2 complexes.[20] Ions are extracted from the ion trap at 5 Hz and are focused into the center of the extraction region of a time-of-flight (TOF) mass spectrometer, where they are irradiated by an intense and wavelength-tunable IR laser pulse from the IR free electron laser FHI FEL.[21] When resonant with a rovibrational transition, the initially internally cold parent ions can absorb one (or more) photon(s), leading to loss of messenger molecules via intramolecular vibrational predissociation. At sufficiently high pulse energies, loss of the more strongly bound CO_2 molecules is also observed.

The TOF intensities of all ions are monitored simultaneously as the FEL wavelength is scanned from 450 to 2400 cm^{-1} in 3 cm^{-1} steps; for each wavelength step, ∼100 TOF traces are acquired and averaged. Over this wavelength range, the FHI FEL has a spectral bandwidth ranging from 2 cm^{-1} fwhm at 450 to 7 cm^{-1} fwhm at 1200 cm^{-1}, and a typical energy output of 10−30 mJ/pulse. Attenuated laser pulses using 12−33% of the full FEL power are employed in a particular spectral window to ensure operation within a linear absorption regime and to avoid saturation. Typically, at least three scans are summed, the photodissociation cross section σ_{IRPD} is determined as described previously,[22,23] and the data obtained in separately scanned ranges are stitched together to obtain the final IRPD spectrum.

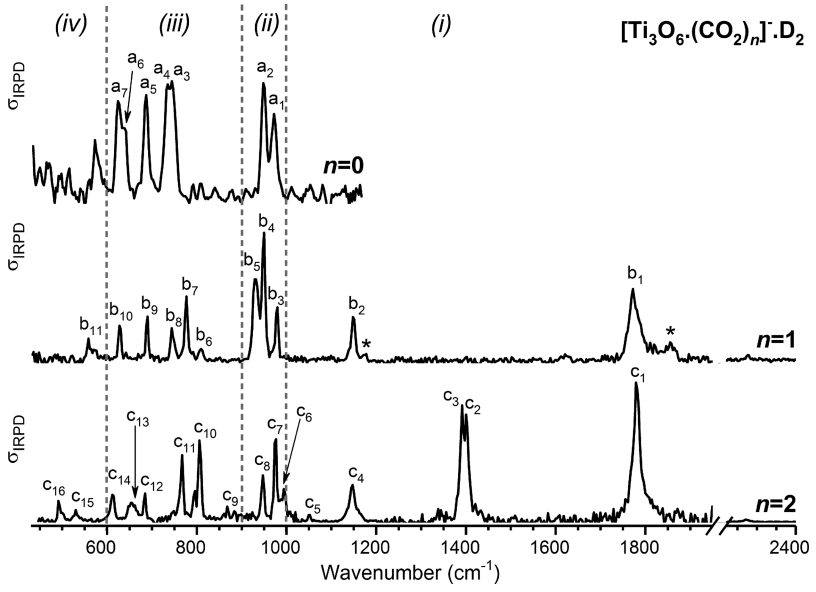

Figure 2. Experimental IRPD spectra of D_2-tagged $[Ti_3O_6(CO_2)_n]^-$ with n = 0, 1 and 2. See Table 2 for band positions and assignments. Four characteristic spectral regions are indicated by the dashed lines: (i) antisymmetric O−C−O stretching modes (>1000 cm^{-1}), (ii) symmetric O−C−O and terminal Ti−O stretching modes (1000−900 cm^{-1}), (iii) stretching modes associated with Ti−O−Ti bridges and O−C−O bending modes (900−600 cm^{-1}), and (iv) low frequency bending, wagging, rocking, and ring breathing modes (<600 cm^{-1}).

DOI: 10.1021/acs.jpcc.8b10724
J. Phys. Chem. C 2019, 123, 8439−8446

Computational Methods. DFT calculations were carried out using the Gaussian 09 (rev. C01) program package[24] to find relative energies, optimized geometries, BSSE-corrected binding energies, harmonic vibrational frequencies, and IR intensities of the lowest-lying $[Ti_3O_6(CO_2)_{n=1-2}]^-$ isomers. We use the range-separated hybrid ωB97X-D functional[25] which includes dispersion interactions. It has been shown to perform well for geometry optimization of transition metal compounds[26] and has provided satisfactory results in our previous work on $[(TiO_2)_{n=2-4}(D_2O)_{m=1-3}]^-$.[12] The aug-cc-pVTZ basis set[27,28] was used for all atoms, with full treatment of all electrons.

Single point CCSD(T) calculations[29−33] of all the lowest lying isomers (for n = 2 aug-cc-pVDZ optimized geometries were taken for CCSD(T) calculation) were performed with the def2-TZVP[34,35] basis set using the TURBOMOLE 6.6 programs.[36] In the search of energetically low-lying structures of bare and D_2-tagged $[Ti_3O_6(CO_2)_{n=1-2}]^-$ isomers, the multicomponent artificial force induced reaction (MC-AFIR) method implemented in the GRRM program was used,[3738] where geometries obtained by the MC-AFIR calculations utilizing the PBE functional and DZP basis set of the SIESTA program[39] were reoptimized at the aforementioned computational level using Gaussian 09 (rev. C01).[24]

3. RESULTS

The experimental IRPD spectra of the D_2-tagged anions $[Ti_3O_6(CO_2)_n]^-$, with n = 0−2, are shown in Figure 2 in the spectral region 450−2400 cm^{-1}. Experimental band positions and band assignments (vide infra) are summarized in Table 1. Based on our previous studies of titanium oxide anions[10,12] and CO_2 adsorption,[40] we group characteristic normal modes into four spectral regions, labeled (i) to (iv) in Figure 2: (i) antisymmetric O−C−O stretching modes (>1000 cm^{-1}), (ii) symmetric O−C−O and terminal Ti−O stretching modes (1000−900 cm^{-1}), (iii) the stretching modes associated with Ti−O−Ti bridges and O−C−O bending modes (900−600 cm^{-1}), and (iv) low frequency bending, wagging, rocking, and ring breathing modes (<600 cm^{-1}). No evidence is found for the IR signature of physisorbed CO_2, which would be above 2000 cm^{-1}, close to the absorption of neutral CO_2 (2349 cm^{-1}).[41]

The IRPD spectrum of D_2-tagged $[Ti_3O_6(CO_2)_n]^-$ for n = 0 has been discussed in detail previously.[10] Briefly, no absorption is observed in the region (i). The two characteristic peaks in region (ii) are the symmetric (a_1, 972 cm^{-1}) and antisymmetric (a_2, 948 cm^{-1}) terminal Ti−O stretching modes. Six vibrational bands that show decreasing IR intensity with decreasing frequency are observed below 750 cm^{-1} and attributed to Ti−O−Ti bridge stretching modes.

The IRPD spectrum for n = 1 (center panel in Figure 2) looks similar to that for n = 0 below 950 cm^{-1}, suggesting that the core structure remains intact upon adsorption of the first CO_2 molecule. The signal-to-noise ratio is slightly better in the present spectra (n = 1, 2) compared to the previously published one (n = 0), mainly a result of improved source conditions.[10] The intense peaks observed above 950 cm^{-1} at 1773 cm^{-1} (b_1), 1144 cm^{-1} (b_2), and 984 cm^{-1} (b_3) signal that CO_2 is preferentially chemisorbed. This particular carbonate stretch pattern, with no absorption in the 1200−1600 cm^{-1} region, fits best with a bridging bidentate carbonate species,[7,8] as discussed in more detail in Section 4. There is a weak feature at 2285 cm^{-1}, indicative of another isomer containing a physisorbed CO_2, but its contribution is negligible.

Table 1. Experimental Band Positions (in cm^{-1}) from the IRPD Spectra of D_2-Tagged $[Ti_3O_6(CO_2)_n]^-$, Shown in Figure 2, and ωB97XD/aug-cc-pVTZ Harmonic Frequencies Scaled by 0.96 (in cm^{-1}) of Isomers 1b (n = 1) and 2a (n = 2), as Well as Band Assignments

n	label	experiment (cm^{-1})	theory (cm^{-1})	assignment
1	b_1	1773	1761	terminal C═O stretch
	b_2	1144	1157	antisym. CO_2 stretch
	b_3	984	1017	sym. CO_2 stretch
	b_4	954	993	terminal Ti−O stretch (sym.)
	b_5	936	965	terminal Ti−O stretch (antisym.)
	b_6	813	748	in-plane CO_3 bend
	b_7	780	726	antisym. Ti−O−Ti ring stretch
	b_8	747	692	antisym. ring breathing
	b_9	693	656	in-plane CO_3 bend
	b_{10}	630	614	O−$(Ti)_3$ stretch
	b_{11}	561	565	O−$(Ti)_3$ bend
2	c_1	1779	1778	terminal C═O stretch
	c_2	1400	1415	antisym. CO_3 stretch
	c_3	1391	1382	antisym. CO_3 stretch
	c_4	1147	1155	antisym. CO_2 stretch
	c_5	1052	1048	sym CO_3 stretch
	c_6	994	1022	terminal Ti−O stretch (sym.)
	c_7	976	994	terminal Ti−O stretch (antisym.)
	c_8	947	954	sym. CO_2 stretch
	c_9	867	874	CO_3 umbrella motion
	c_{10}	806	776	antisym. Ti−O−Ti ring stretch
	c_{11}	767	756	in-plane CO_2 bend
	c_{12}	684	672	antisym. Ti−O−Ti ring stretch
	c_{13}	653	651	in-plane CO_2/CO_3 bend
	c_{14}	612	602	sym. Ti−O−Ti ring stretch
	c_{15}	530	530	antisym. ring breathing
	c_{16}	491	484	antisym. ring breathing

The IRPD spectrum for n = 2 (bottom panel in Figure 2) shows similarities to the n = 1 spectrum over large parts of the spectral range. The carbonate stretching bands c_1, c_4, and c_6 in the n = 2 spectrum are found nearly unshifted from the positions in the n = 1 spectrum, where they correspond to bands b_1, b_2, and b_3. The persistence of these bands supports an identical bridging bidentate binding motif for one of the two CO_2 molecules in the n = 2 species. There are, however, two new, closely spaced features at 1400 cm^{-1} (c_2) and 1391 cm^{-1} (c_3) that cannot be attributed to any of the known CO_2 binding motifs,[7,8] including those proposed in a recent computational study on neutral $Ti_3O_6(CO_2)_n$ clusters.[15]

4. ANALYSIS AND DISCUSSION

In order to assign the IRPD spectra, we performed geometry optimizations and harmonic frequency calculations using DFT. The ωB97XD/aug-cc-pVTZ relative electronic energies ΔE_{DFT} and zero-point energy (ZPE) corrected relative energies $\Delta E_{0,DFT}$ are listed in Table 2. To obtain more accurate electronic energies, we also calculated CCSD(T)/def2-TZVP single-point energies $\Delta E_{CCSD(T)}$ at the optimized ωB97XD/aug-cc-pVTZ geometry; these are also listed in Table 2. The six

DOI: 10.1021/acs.jpcc.8b10724
J. Phys. Chem. C 2019, 123, 8439−8446

Table 2. ωB97XD/aug-cc-pVTZ Relative Electronic Energies ΔE_{DFT} and ZPE-Corrected Relative Energies $\Delta E_{0,DFT}$ of the Lowest-Energy Minimum-Energy Isomers of $[Ti_3O_6\ (CO_2)_{n=1,2}]^-$[a]

n	isomer	ΔE_{DFT}[b]	$\Delta E_{0,DFT}$[c]	$\Delta E_{CCSD(T)}$[b]	$\Delta E_{0,CCSD(T)/DFT}$[c]
1	**1a**	0.0	0.0	0.0	0.0
	1b	19.1	18.0	0.0	−0.8
	1c	12.0	11.9	10.5	11.2
	1d	37.4	39.2	81.7	84.4
	1e	45.1	38.2	156.0	149.9
	1f	53.4	46.2	130.2	123.8
2	**2a**	0.0	0.0	0.0	0.0
	2b	18.5	17.8	14.9	14.2
	2c	24.5	24.2	41.8	41.6
	2d	32.5	30.6	27.4	25.4
	2e	39.2	38.8	75.4	75.1
	2f	41.4	40.1	47.5	46.2

[a]CCSD(T)/def2-TZVP relative electronic energies $\Delta E_{CCSD(T)}$ at the DFT minimum-energy geometry and ZPE-corrected relative electronic energies $\Delta E_{0,CCSD(T)/DFT}$ using the DFT ZPE-correction are also shown. All energies are given in kJ/mol. [b]Absolute energies: −3189.03837 au (**1a**, DFT), −3182.85095 au (**1a**, CCSD(T)), −3377.67800 au (**2a**, DFT), −3370.61920 au (**2a**, CCSD(T)). [c]Zero-point-energy (ZPE) determined from ωB97XD/aug-cc-pVTZ harmonic vibrational frequencies.

lowest minimum-energy structures for n = 1 and n = 2 are shown in Figure 3. The isomers are labeled with ***nx***, where ***n*** is the number of CO_2 molecules adsorbed to $Ti_3O_6^-$ and ***x*** = **a**, **b**, **c**, ... indicates the energetic ordering. See Tables 2 and S3 for the isomer energies and Figures S2 and S3 for the harmonic IR spectra of all the considered isomers.

For $[Ti_3O_6.CO_2]^-$, we considered the six structures (**1a**−**1f**) shown in Figure 3. Their relative energies are listed in Table 2. Chemisorption, that is, carbonate formation (**1a**−**1d**), is preferred over physisorption, with a counterpoise-corrected DFT CO_2 binding energy of 139 kJ/mol (**1a**). Note that the physisorbed complexes (**1e**, **1f**) are predicted to lie even higher in energy when the CCSD(T) energies are considered (see Table 2). Structure **1a** represents the global minimum-energy structure using DFT. Structure **1b** is predicted to be 19 kJ/mol higher in energy. However, when the CCSD(T) energies are considered, structures **1a** and **1b** are nearly isoenergetic, with **1b** predicted only +0.3 kJ/mol higher in energy. Moreover, when the harmonic vibrational ZPEs from DFT are combined with the CCSD(T) electronic energies, the energetic ordering is reversed and **1b** is indeed slightly favored by 0.8 kJ/mol. Both of these structures exhibit carbonate binding motifs, but in different binding environments and with different formal charges on the carbonate moiety: −1.039 |e| (**1a**) versus −1.126 |e| (**1b**) (see Figure S6 and Table S1). Structure **1a** contains a tridentate, quasi-symmetric carbonate moiety, $(C(-O)_3)^{2-}$, that exhibits three similar C−O bonds (~131 pm, see SI) and forms three Ti−O bonds, one to each of the three Ti centers. On the other hand, **1b** contains an asymmetric tridentate carbonate moiety, $(O{=}C(-O)_2)^{2-}$, that involves a bridging O atom and only two Ti-centers. The higher energy chemisorbed structures involve an asymmetric bidentate carbonate species bound to a single Ti-center (**1c**, $\Delta E_{CCSD(T)}$ = 11 kJ/mol) and a quasi-symmetric tetradentate carbonate species bound to two Ti-centers involving a bridging O atom (**1d**, +82 kJ/mol). Dixon and co-workers[15] find structures similar to **1b** to **1d** for neutral chemisorbed

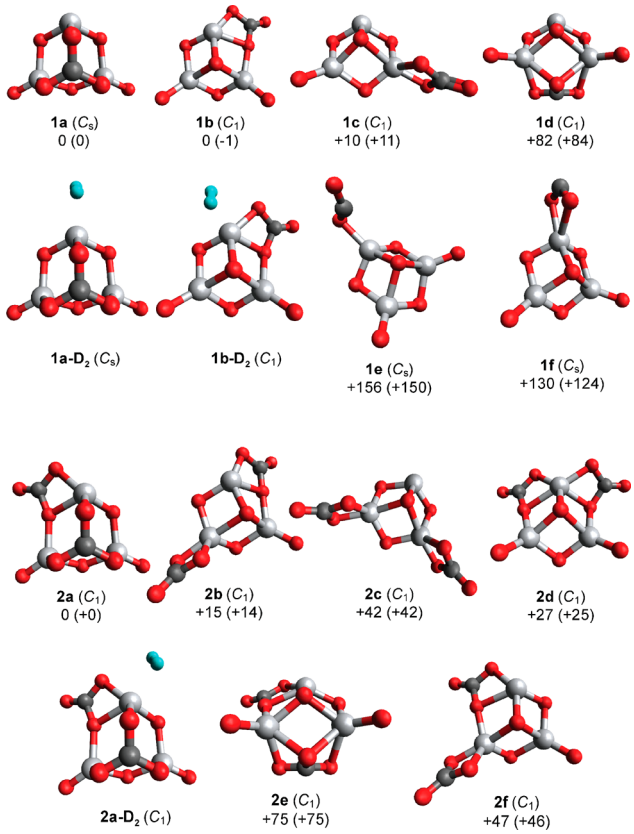

Figure 3. ωB97X-D/aug-cc-pVTZ minimum-energy structures, symmetry (in parentheses) and relative CCSD(T) single-point energy (in kJ·mol^{-1}) of energetically low-lying $[Ti_3O_6\ (CO_2)_{n=1,2}]^-$ isomers. The ZPE-corrected energies are given in parentheses. The isomers are labeled with ***nx***, where ***n*** is the number of CO_2 molecules adsorbed and ***x*** = **a**, **b**, **c**, ..., which indicates the energetic ordering. Atoms in gray represent Ti, dark gray represents C, red represents O, and blue represents H. The structures of D_2-tagged species for **1a**, **1b**, and **2a** are also shown.

$[Ti_3O_6(CO_2)]$ clusters of which the neutral structure corresponding to **1d** was found to be the lowest in energy. Interestingly, they did not consider the tridendate symmetric carbonate motif of **1a**. We determined the optimized geometry of the neutral analogue of **1a** and find that it lies 20 kJ/mol above the **1d** analogue using DFT (see Table S1). However, when the CCSD(T) energies are considered, the order is reversed; the **1a** analogue is predicted 11 kJ/mol below the **1d** analogue and thus is likely the ground state structure of neutral $[Ti_3O_6(CO_2)]$. Formation of the physisorbed species **1e** (+130 kJ/mol) and **1f** (+156 kJ/mol) is less favorable compared to the corresponding neutral clusters and contain bent CO_2 moieties (see SI for geometric parameters), indicating partial charge transfer to the CO_2.

Messenger-tagging with D_2 also plays a significant role for the energetic ordering of the isomers. We calculated counterpoise-corrected D_2 binding energies for **1a**·D_2 and **1b**·D_2 and find that **1b** (21 kJ/mol) binds D_2 more than twice as strong as **1a** (9.0 kJ/mol). This is presumably due to the higher positive atomic charge on the corresponding Ti atom in **1b** (0.86 |e|) versus **1a** (0.59 |e|). Hence, messenger tagging favors the formation of **1b**·D_2.

For n = 2, we considered the six structures shown in Figure 3. Their relative DFT and CCSD(T) energies are listed in Table 2. Independent of the computational method used, **2a** is

DOI: 10.1021/acs.jpcc.8b10724
J. Phys. Chem. C 2019, 123, 8439−8446

predicted to lie lowest in energy followed by **2b**, which lies about 15 kJ/mol higher. Structure **2a** consists of two chemisorbed CO_2 molecules in the form of a bidentate (**1b**) and tridentate (**1a**) bridged carbonate, the two most stable n = 1 motifs. Structure **2b** corresponds to the combination of the **1b**/**1c** motifs, while the higher energy isomers **2d** (+27 kJ/mol), **2c** (+42 kJ/mol), and **2e** (+75 kJ/mol) then represent the **1b**/**1b**, **1c**/**1c**, and **1b**/**1d** combinations, respectively. Structure **2f** (+48 kJ/mol) exhibits similar CO_2 binding motifs as **2b**, but here the two carbonate groups share a Ti^{4+} center.

In order to assign the IRPD spectra of the D_2-tagged $[Ti_3O_6(CO_2)_n]^-$ anions with n = 1 and 2, we compare them to the calculated harmonic spectra of the three lowest energy isomers (without tag) in Figures 4 and 5, respectively (see Figures S2 and S3 for a comparison to the spectra of all isomers, also including isomers with D_2 tag). For n = 1 (see Figure 4), we find the best agreement of the experimental D_2-loss IRPD spectrum with the simulated spectrum of **1b**. It reproduces all of the observed bands b_1 to b_{11} satisfactorily (see Table 1). The three absorption bands b_1 (1773 cm^{-1}), b_2 (1144 cm^{-1}), and b_3 (984 cm^{-1}) are assigned to the terminal C═O (1761 cm^{-1}), antisymmetric CO_2 (1157 cm^{-1}), and symmetric CO_2 (1017 cm^{-1}) stretching modes, respectively, of the bridging bidentate carbonate moiety. Bands b_4 (954 cm^{-1}) and b_5 (936 cm^{-1}) correspond to the symmetric (993 cm^{-1}) and antisymmetric (965 cm^{-1}) combinations of the terminal Ti−O stretching modes, followed by CO_3 bending (b_6, b_9) and Ti−O−Ti stretching and bending modes at lower energies. Note that the weak features at 1855 and 1174 cm^{-1} (marked with an asterisk in Figure 2) are not reproduced by the harmonic spectrum and we therefore attribute them to

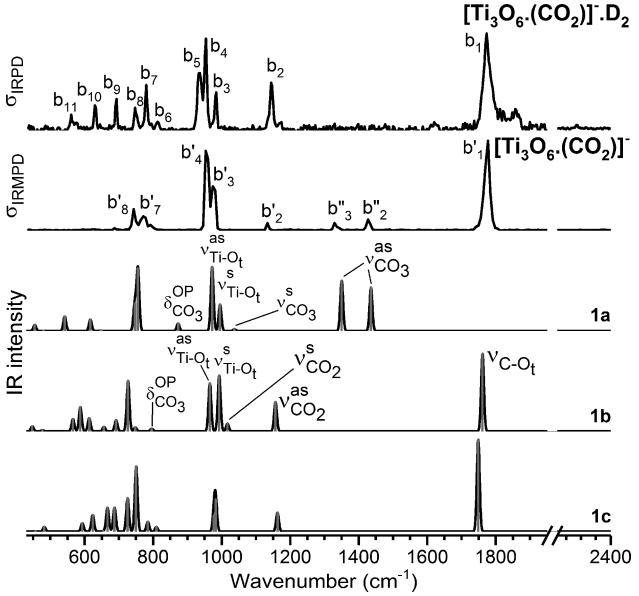

Figure 4. Experimental IRPD and IRMPD spectra of D_2-tagged $[Ti_3O_6(CO_2)]^-$ and calculated IR spectra of the three energy isomers (**1a**−**1c**) of the untagged anions. The IRPD spectrum (top panel), measured with an attenuated (14%) laser beam, shows the D_2-loss channel, while the IRMPD spectrum (second panel from top), measured with a nonattenuated laser beam, shows the CO_2-loss channel. The calculated IR spectra (lower panels), derived from ωB97XD/aug-cc-pVTZ harmonic frequencies (scaled by 0.96) and intensities, are plotted with sticks (gray) and a 10 cm^{-1} fwhm Gaussian line shape convolution. See Table 1 for band assignments.

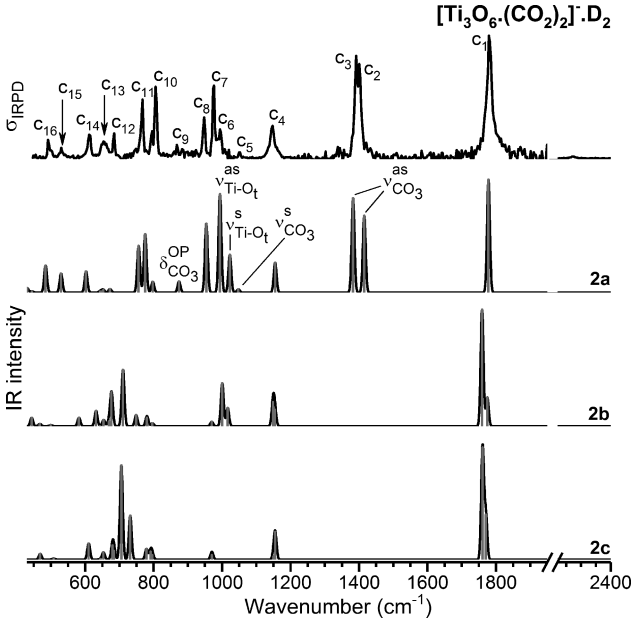

Figure 5. Experimental IRPD spectra of D_2-tagged $[Ti_3O_6(CO_2)_2]^-$ (top panel) and calculated IR spectra (lower panels) of the three low-energy isomers (**2a**-**2c**) of the untagged anions. The calculated IR spectra, derived from ωB97XD/aug-cc-pVTZ harmonic frequencies (scaled by 0.96) and intensities, are plotted with sticks (gray) and a 10 cm^{-1} fwhm Gaussian line shape convolution. See Table 1 for band assignments.

excitation of antisymmetric CO_2 stretching mode/triply coordinated O atom stretching mode and carbonate bending mode/ring breathing mode combination bands, respectively. The spectrum of **1c**, on the other hand, does not reproduce the characteristic triplet b_3−b_5 around 1000 cm^{-1}, because one of the Ti═O sites is occupied. The spectrum of **1a** exhibits two characteristic antisymmetric stretching modes of the symmetrically bound carbonate species at 1436 and 1350 cm^{-1}, which are not observed in the D_2-loss channel.

Interestingly, we do find evidence for the population of (bare) **1a** when monitoring the CO_2-loss channel as part of IRMPD measurements using higher pulse energies (~8 vs 1 mJ). In addition to the features previously attributed to **1b**, the corresponding IRMPD spectrum (see second trace from top in Figure 4) exhibits two weaker peaks at 1427 (b_2'') and 1329 cm^{-1} (b_3''), which we assign to the two antisymmetric stretching modes of the tridendate carbonate in **1a**. This observation confirms that **1a** lies close in energy to **1b** in the absence of tagging and both are formed and present initially in the ion trap, but subsequent D_2-tagging then favors the formation **1b**-D_2 over **1a**-D_2.

The IRPD spectrum of the n = 2 cluster is compared to the harmonic spectra of the three lowest energy isomers in Figure 5. Only the spectrum of the lowest energy isomer **2a** reproduces the characteristic IR signature in the C−O stretching region. The four bands at 1779 (c_1), 1400 (c_2), 1391 (c_3) and 1147 cm^{-1} (c_4) are assigned to the terminal C═O (1778 cm^{-1}) and antisymmetric CO_2 stretch (1155 cm^{-1}) of the bidentate carbonate as well as the two antisymmetric CO_3 stretches (1415 and 1382 cm^{-1}) of the tridentate carbonate. Note that the calculated splitting of the antisymmetric CO_3 stretches of 33 cm^{-1} for the untagged cluster (spectrum **2a** in Figure 5) is substantially larger than the experimental value of 9 cm^{-1} (for the tagged cluster), but is

DOI: 10.1021/acs.jpcc.8b10724
J. Phys. Chem. C 2019, 123, 8439−8446

reduced to 2 cm^{-1} when D_2-tagging is explicitly considered (see Figure S3). This is the only band that shows such a pronounced messenger-tag induced shift. The bands at lower energies can then be assigned as follows. Bands c_5 (1052 cm^{-1}) and c_8 (947 cm^{-1}) are the symmetric CO_3 (1048 cm^{-1}) and CO_2 (954 cm^{-1}) stretches of the tridentate and bidentate bridging carbonates, respectively. The symmetric (1022 cm^{-1}) and antisymmetric (994 cm^{-1}) combinations of the terminal Ti−O stretches correspond to bands c_6 (994 cm^{-1}) and c_7 (976 cm^{-1}), followed by Ti−O−Ti ring stretching (c_{10},c_{12}), CO_3/CO_2 bending modes (c_9,c_{11},c_{13}), and Ti−O−Ti ring breathing modes (c_{14}-c_{16}) at lower energies (see Table 1). The spectra of **2b** and **2c**, on the other hand, cannot recover the experimental spectrum, in particular the characteristic doublet of the tridentate carbonate moiety around 1400 cm^{-1} (c_2, c_3) is absent from these spectra.

The similarities in the IRPD spectra of D_2-tagged $[Ti_3O_6(CO_2)_{0-2}]^-$ anions show that addition of up to two CO_2 molecules to $Ti_3O_6^-$ leads to local perturbations rather than overall structural changes. For example, the two terminal Ti═O bonds remain intact and slightly increase in bond strength upon CO_2 addition, indicated by a small, but consistent, blue-shift of the corresponding stretching modes from 970/948 cm^{-1} (n = 0) to 984/954 cm^{-1} in the n = 1 cluster and 994/976 cm^{-1} in the n = 2 cluster, concomitant with a predicted shortening of the terminal Ti−O bonds from 164 pm (n = 0) to 162 pm (n = 2). Similarly, the two stretching modes associated with the bidentate carbonate species are also slightly blue-shifted from 1773/1144 cm^{-1} (n = 1) to 1779/1147 cm^{-1} (n = 2). The spectral changes in regions (iii) and (iv) (<900 cm^{-1}) are slightly more pronounced, but also not dramatic. Finally, calculation of the spin density for the n = 0−2 anions (see Figure S5) confirms that the localized, unpaired electron remains nearly unperturbed upon CO_2 adsorption. On the other hand, D_2-tagging leads to more substantial effects, for example, the symmetric CO_2 stretch in the spectrum of **1b** is red-shifted by 61 cm^{-1} and its IR intensity increases by a factor of 6 (from 99 to 626 km/mol) upon D_2-tagging (see Figure S2) as a result of electron delocalization from the Ti^{3+} center to the D_2 molecule.

5. CONCLUSIONS

In summary, we find that the first two CO_2 molecules adsorb chemically to $Ti_3O_6^-$, leaving the unpaired electron largely unperturbed. CO_2 activation in this case involves the incorporation of a formally doubly negatively charged, either doubly or triply coordinated O atom to form a bidentate or tridentate bridging carbonate dianion (CO_3^{2-}), respectively. The bidentate binding motif described here is well-known from CO_2 adsorption studies on TiO_2 anatase surfaces[7,8,13,14] and has also been predicted as a particular stable motif for CO_2 adsorption on neutral gas phase titanium oxide clusters.[15] The tridentate binding motif is identified here experimentally for the first time and exhibits a characteristic IR signature in the form of an intense doublet of peaks near 1400 cm^{-1}, which correspond to two antisymmetric carbonate stretching modes.

The present results have several implications for understanding CO_2 activation/conversion in general and CO_2 adsorption at titania interfaces in particular. For example, the characterization of the role of bicarbonate (HCO_3^-) species in such processes using IR spectroscopy may require additional scrutiny, since the characteristic doublet of the tridentate carbonate binding motif lies in the same spectral region that has typically been attributed to HCO_3^-.[8,14] Moreover, recent DFT calculations suggest that a tridentate binding motif plays a central role in the oxygen exchange mechanism on a defective anatase surface.[42] However, the prediction of the reaction barriers for such rather complex systems using DFT depends intimately on the specific value of the Hubbard U correction used to describe the on-site Coulomb interaction.[43,44] Gas phase clusters such as those studied here represent ideal model systems to accurately test more such approximate computational methods, since smaller clusters are amenable to higher level calculations.[19,45,46]

The present study also demonstrates the high potential of calculations based on the AFIR method for investigation of chemical reactions on small atomic clusters. In future IRPD studies, we will try to obtain a molecular level understanding of how water coadsorption influences CO_2 activation in these model systems and how this ultimately can be exploited for the catalytic conversion of CO_2 to value-added chemicals.

■ ASSOCIATED CONTENT

Supporting Information

The Supporting Information is available free of charge on the ACS Publications website at DOI: 10.1021/acs.jpcc.8b10724.

Quadrupole mass spectra; experimental spectra compared to computed spectra for all the isomers; additional possible isomers, spin densities, and NBO charges; isomer energies; Cartesian atomic coordinates of all calculated isomers (PDF).

■ AUTHOR INFORMATION

Corresponding Authors

*E-mail: knut.asmis@uni-leipzig.de.
*E-mail: dneumark@berkeley.edu.
*E-mail: lyalin.andrey@nims.go.jp.

ORCID

Satoshi Maeda: 0000-0001-8822-1147
Tetsuya Taketsugu: 0000-0002-1337-6694
Wieland Schöllkopf: 0000-0003-0564-203X
Knut R. Asmis: 0000-0001-6297-5856

Present Address

[‖]JILA, National Institute of Standards and Technology, Boulder, Colorado 80305, U.S.A.

Notes

The authors declare no competing financial interest.

■ ACKNOWLEDGMENTS

This work has been supported by the German Research Foundation (DFG) within the CRC 1109 "Metal Oxide−Water Systems". X.S. thanks the Alexander-von-Humboldt Foundation for a postdoctoral research fellowship. M.L.W. thanks the National Science Foundation for a graduate research fellowship. D.M.N. thanks the Air Force Office of Scientific Research for funding this research (No. FA9550-16-1-0097). M.G., S.M., T.T., and A.L. are grateful for financial support from the programs of the Ministry of Education, Culture, Sports, Science and Technology (MEXT, Japan) on the "Development of Environmental Technology using Nanotechnology" and "Priority Issue on Post-K computer" (development of new fundamental technologies for high-efficiency energy creation, conversion/storage and use). Institute for Chemical Reaction Design and Discovery

DOI: 10.1021/acs.jpcc.8b10724
J. Phys. Chem. C 2019, 123, 8439−8446

(ICRD) was established by World Premier International Research Initiative (WPI), MEXT, Japan. A.L. and T.T. gratefully acknowledge the financial support of JSPS KAKENHI Grant Nos. 15K05387 and 16KT0047, respectively.

REFERENCES

(1) Habisreutinger, S. N.; Schmidt-Mende, L.; Stolarczyk, J. K. Photocatalytic reduction of CO_2 on TiO_2 and other semiconductors. *Angew. Chem., Int. Ed.* **2013**, *52*, 7372−7408.
(2) Civiš, S.; Ferus, M.; Knížek, A.; Kubelík, P.; Kavan, L.; Zukalová, M. Photocatalytic transformation of CO_2 to CH_4 and CO on acidic surface of TiO_2 anatase. *Opt. Mater.* **2016**, *56*, 80−83.
(3) Linsebigler, A. L.; Lu, G.; Yates, J. T. Photocatalysis on TiO_2 surfaces: Principles, mechanisms, and selected results. *Chem. Rev.* **1995**, *95*, 735−758.
(4) Thompson, T. L.; Yates, J. T. Surface science studies of the photoactivation of TiO_2: New photochemical processes. *Chem. Rev.* **2006**, *106*, 4428−4453.
(5) Guo, Q.; Zhou, C.; Ma, Z.; Ren, Z.; Fan, H.; Yang, X. Elementary photocatalytic chemistry on TiO_2 surfaces. *Chem. Soc. Rev.* **2016**, *45*, 3701−3730.
(6) Martra, G. Lewis acid and base sites at the surface of microcrystalline TiO_2 anatase: relationships between surface morphology and chemical behaviour. *Appl. Catal., A* **2000**, *200*, 275−285.
(7) Liao, L. F.; Lien, C. F.; Shieh, D. L.; Chen, M. T.; Lin, J. L. FTIR study of adsorption and photoassisted oxygen isotopic exchange of carbon monoxide, carbon dioxide, carbonate, and formate on TiO_2. *J. Phys. Chem. B* **2002**, *106*, 11240−11245.
(8) Mino, L.; Spoto, G.; Ferrari, A. M. CO_2 capture by TiO_2 anatase surfaces: A combined DFT and FTIR study. *J. Phys. Chem. C* **2014**, *118*, 25016−25026.
(9) He, H.; Zapol, P.; Curtiss, L. A. A theoretical study of CO_2 anions on anatase (101) surface. *J. Phys. Chem. C* **2010**, *114*, 21474−21481.
(10) Weichman, M. L.; Song, X. W.; Fagiani, M. R.; Debnath, S.; Gewinner, S.; Schöllkopf, W.; Neumark, D. M.; Asmis, K. R. Gas phase vibrational spectroscopy of cold $(TiO_2)_n^-$ (n = 3−8) clusters. *J. Chem. Phys.* **2016**, *144*, 124308.
(11) Song, X. W.; Fagiani, M. R.; Debnath, S.; Gao, M.; Maeda, S.; Taketsugu, T.; Gewinner, S.; Schöllkopf, W.; Asmis, K. R.; Lyalin, A. Excess charge driven dissociative hydrogen adsorption on $Ti_2O_4^-$. *Phys. Chem. Chem. Phys.* **2017**, *19*, 23154−23161.
(12) Weichman, M. L.; Debnath, S.; Kelly, J. T.; Gewinner, S.; Schöllkopf, W.; Neumark, D. M.; Asmis, K. R. Dissociative water adsorption on gas-phase titanium dioxide cluster anions probed with infrared photodissociation spectroscopy. *Top. Catal.* **2018**, *61*, 92−105.
(13) Freund, H. J.; Roberts, M. W. Surface chemistry of carbon dioxide. *Surf. Sci. Rep.* **1996**, *25*, 225−273.
(14) Su, W. G.; Zhang, J.; Feng, Z. C.; Chen, T.; Ying, P. L.; Li, C. Surface phases of TiO_2 nanoparticles studied by UV Raman spectroscopy and FT-IR spectroscopy. *J. Phys. Chem. C* **2008**, *112*, 7710−7716.
(15) Flores, L. A.; Murphy, J. G.; Copeland, W. B.; Dixon, D. A. Reaction of CO_2 with groups 4 and 6 transition metal oxide clusters. *J. Phys. Chem. A* **2017**, *121*, 8719−8727.
(16) Dodson, L. G.; Thompson, M. C.; Weber, J. M. Interactions of molecular titanium oxides TiO_x (x = 1−3) with carbon dioxide in cluster anions. *J. Phys. Chem. A* **2018**, *122*, 6909−6917.
(17) Goebbert, D. J.; Meijer, G.; Asmis, K. R. 10K ring electrode trap - tandem mass spectrometer for infrared spectroscopy of mass selected ions. *AIP Conf. Proc.* **2008**, *1104*, 22−29.
(18) Goebbert, D. J.; Garand, E.; Wende, T.; Bergmann, R.; Meijer, G.; Asmis, K. R.; Neumark, D. M. Infrared spectroscopy of the microhydrated nitrate ions $NO_3^-(H_2O)_{1-6}$. *J. Phys. Chem. A* **2009**, *113*, 7584−7592.
(19) Fagiani, M. R.; Song, X.; Debnath, S.; Gewinner, S.; Schöllkopf, W.; Asmis, K. R.; Bischoff, F. A.; Müller, F.; Sauer, J. Dissociative water adsorption by $Al_3O_4^+$ in the gas phase. *J. Phys. Chem. Lett.* **2017**, *8*, 1272−1277.
(20) Brümmer, M.; Kaposta, C.; Santambrogio, G.; Asmis, K. R. Formation and photodepletion of cluster ion-messenger atom complexes in a cold ion trap: Infrared spectroscopy of VO^+, VO_2^+, and VO_3^+. *J. Chem. Phys.* **2003**, *119*, 12700−12703.
(21) Schöllkopf, W.; Gewinner, S.; Junkes, H.; Paarmann, A.; von Helden, G.; Bluem, H.; Todd, A. M. M. The new IR and THz FEL facility at the Fritz Haber Institute in Berlin. *Proc SPIE*, 2015, *9512*, 95121L.
(22) Heine, N.; Asmis, K. R. Cryogenic ion trap vibrational spectroscopy of hydrogen-bonded clusters relevant to atmospheric chemistry. *Int. Rev. Phys. Chem.* **2015**, *34*, 1−34.
(23) Heine, N.; Asmis, K. R. Cryogenic ion trap vibrational spectroscopy of hydrogen-bonded clusters relevant to atmospheric chemistry (vol 34, pg 1, 2015). *Int. Rev. Phys. Chem.* **2016**, *35*, 507−507.
(24) Frisch, M. J.; Trucks, G. W.; Schlegel, H. B.; Scuseria, G. E.; Robb, M. A.; Cheeseman, J. R.; Scalmani, G.; Barone, V.; Mennucci, B.; Petersson, G. A.; et al. *Gaussian 09*, version D01; Gaussian, Inc.: Wallingford, CT, U.S.A., 2009.
(25) Chai, J.-D.; Head-Gordon, M. Long-range corrected hybrid density functionals with damped atom-atom dispersion corrections. *Phys. Chem. Chem. Phys.* **2008**, *10*, 6615−6620.
(26) Minenkov, Y.; Singstad, A.; Occhipinti, G.; Jensen, V. R. The accuracy of DFT-optimized geometries of functional transition metal compounds: a validation study of catalysts for olefin metathesis and other reactions in the homogeneous phase. *Dalton Trans.* **2012**, *41*, 5526−5541.
(27) Kendall, R. A.; D, T. H., Jr.; Harrison, R. J. Electron affinities of the first-row atoms revisited. Systematic basis sets and wave functions. *J. Chem. Phys.* **1992**, *96*, 6796−6806.
(28) Davidson, E. R. Comment on "Comment on Dunning's correlation-consistent basis sets. *Chem. Phys. Lett.* **1996**, *260*, 514−518.
(29) Noga, J.; Bartlett, R. J. The full CCSDT model for molecular electronic structure. *J. Chem. Phys.* **1987**, *86*, 7041−7050.
(30) Urban, M.; Noga, J.; Cole, S. J.; Bartlett, R. J. Towards a full CCSDT model for electron correlation. *J. Chem. Phys.* **1985**, *83*, 4041−4046.
(31) Stanton, J. F. Why CCSD(T) works: a different perspective. *Chem. Phys. Lett.* **1997**, *281*, 130−134.
(32) Raghavachari, K.; Trucks, G. W.; Pople, J. A.; Head-Gordon, M. A fifth-order perturbation comparison of electron correlation theories. *Chem. Phys. Lett.* **1989**, *157*, 479−483.
(33) Bartlett, R. J.; Musiał, M. Coupled-cluster theory in quantum chemistry. *Rev. Mod. Phys.* **2007**, *79*, 291−352.
(34) Weigend, F.; Ahlrichs, R. Balanced basis sets of split valence, triple zeta valence and quadruple zeta valence quality for H to Rn: Design and assessment of accuracy. *Phys. Chem. Chem. Phys.* **2005**, *7*, 3297−3305.
(35) Hellweg, A.; Hättig, C.; Höfener, S.; Klopper, W. Optimized accurate auxiliary basis sets for RI-MP2 and RI-CC2 calculations for the atoms Rb to Rn. *Theor. Chem. Acc.* **2007**, *117*, 587−597.
(36) Ahlrichs, R.; Bär, M.; Häser, M.; Horn, H.; Kölmel, C. Electronic structure calculations on workstation computers: The program system turbomole. *Chem. Phys. Lett.* **1989**, *162*, 165−169.
(37) Maeda, S.; Ohno, K.; Morokuma, K. Systematic exploration of the mechanism of chemical reactions: the global reaction route mapping (GRRM) strategy using the ADDF and AFIR methods. *Phys. Chem. Chem. Phys.* **2013**, *15*, 3683−3701.
(38) Maeda, S.; Harabuchi, Y.; Sumiya, Y.; Takagi, M.; Suzuki, K.; Hatanaka, M.; Osada, Y.; Taketsugu, T.; Morokuma, K.; Ohno, K. GRRM, a developmental version at Hokkaido University; https://afir.sci.hokudai.ac.jp (accessed 29 August, 2018).

DOI: 10.1021/acs.jpcc.8b10724
J. Phys. Chem. C 2019, 123, 8439−8446

(39) José, M. S.; Emilio, A.; Julian, D. G.; Alberto, G.; Javier, J.; Pablo, O.; Daniel, S.-P. The SIESTA method for ab initio order- N materials simulation. *J. Phys.: Condens. Matter* **2002**, *14*, 2745.
(40) Miller, G. B. S.; Esser, T. K.; Knorke, H.; Gewinner, S.; Schoellkopf, W.; Heine, N.; Asmis, K. R.; Uggerud, E. Spectroscopic identification of a bidentate binding motif in the anionic magnesium-CO_2 complex ($[ClMgCO_2]^-$). *Angew. Chem., Int. Ed.* **2014**, *53*, 14407−14410.
(41) Shimanouchi, T. *Tables of molecular vibrational frequencies consolidated*; National Bureau of Standards, 1972; Vol. *1*, pp 1−160.
(42) Sorescu, D. C.; Civiš, S.; Jordan, K. D. Mechanism of oxygen exchange between CO_2 and TiO_2(101) anatase. *J. Phys. Chem. C* **2014**, *118*, 1628−1639.
(43) Anisimov, V. I.; Zaanen, J.; Andersen, O. K. Band theory and Mott insulatoras - Hubbard-U instead of Stoner-I. *Phys. Rev. B: Condens. Matter Mater. Phys.* **1991**, *44*, 943−954.
(44) Dudarev, S. L.; Botton, G. A.; Savrasov, S. Y.; Humphreys, C. J.; Sutton, A. P. Electron-energy-loss spectra and the structural stability of nickel oxide: An LSDA+U study. *Phys. Rev. B: Condens. Matter Mater. Phys.* **1998**, *57*, 1505−1509.
(45) Burow, A. M.; Wende, T.; Sierka, M.; Wlodarczyk, R.; Sauer, J.; Claes, P.; Jiang, L.; Meijer, G.; Lievens, P.; Asmis, K. R. Structures and vibrational spectroscopy of partially reduced gas-phase cerium oxide clusters. *Phys. Chem. Chem. Phys.* **2011**, *13*, 19393−19400.
(46) Jiang, L.; Wende, T.; Claes, P.; Bhattacharyya, S.; Sierka, M.; Meijer, G.; Lievens, P.; Sauer, J.; Asmis, K. R. Electron distribution in partially reduced mixed metal oxide systems: Infrared spectroscopy of $Ce_mV_nO_o^+$ gas phase clusters. *J. Phys. Chem. A* **2011**, *115*, 11187−11192.

DOI: 10.1021/acs.jpcc.8b10724
J. Phys. Chem. C 2019, 123, 8439−8446